ACS APPLIED MATERIALS & INTERFACES

Research Article

www.acsami.org

Thermal Evaporation and Characterization of Sb_2Se_3 Thin Film for Substrate Sb_2Se_3/CdS Solar Cells

Xinsheng Liu,[†,‡,§] Jie Chen,[†,‡,§] Miao Luo,[†,‡] Meiying Leng,[†,‡] Zhe Xia,[†,‡] Ying Zhou,[†,‡] Sikai Qin,[†,‡] Ding-Jiang Xue,[†,‡] Lu Lv,[⊥] Han Huang,[⊥] Dongmei Niu,[⊥] and Jiang Tang*[,†,‡]

[†]Wuhan National Laboratory for Optoelectronics (WNLO) and [‡]School of Optical and Electronic Information, Huazhong University of Science and Technology, Wuhan 430074, Hubei, P. R. China

[⊥]Institute of Super-microstructure and Ultrafast Process in Advanced Materials, School of Physics and Electronics, The Central South University, Changsha, Hunan 410083, P. R. China

Supporting Information

ABSTRACT: Sb_2Se_3 is a promising absorber material for photovoltaic cells because of its optimum band gap, strong optical absorption, simple phase and composition, and earth-abundant and nontoxic constituents. However, this material is rarely explored for photovoltaic application. Here we report Sb_2Se_3 solar cells fabricated from thermal evaporation. The rationale to choose thermal evaporation for Sb_2Se_3 film deposition was first discussed, followed by detailed characterization of Sb_2Se_3 film deposited onto FTO with different substrate temperatures. We then studied the optical absorption, photosensitivity, and band position of Sb_2Se_3 film, and finally a prototype photovoltaic device FTO/Sb_2Se_3/CdS/ZnO/ZnO:Al/Au was constructed, achieving an encouraging 2.1% solar conversion efficiency.

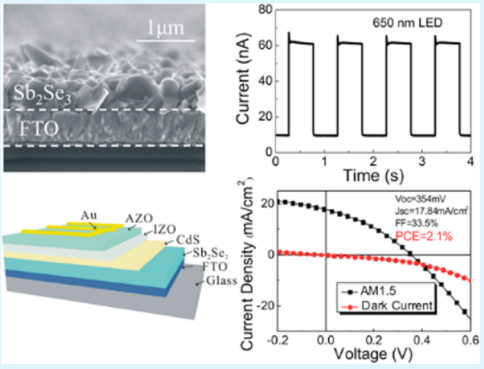

KEYWORDS: *Sb_2Se_3, thermal evaporation, thin film, solar cells*

1. INTRODUCTION

Thin-film solar cells have made impressive improvements in device efficiency recently, with copper indium gallium selenide (CIGS) and cadmium telluride (CdTe) solar cells achieving certified solar energy conversion efficiencies of 20.8[1] and 20.4%,[2] respectively. However, because of the toxicity of Cd, the scarcity of In and Te, and high price of In and Ga, tera-watt scale application of these thin-film solar cells might be restricted. Therefore, earth-abundant, nontoxic, and low-cost materials should be explored for high-efficiency solar cells. Copper zinc tin sulfoselenide (CZTSSe) is such a promising absorber candidate intensively researched and has achieved a 12.6% conversion efficiency through hydrazine-based solution process.[3] Because hydrazine is toxic, low-toxicity solution process is developed.[4,5] However, CZTSSe is a multinary compound, stringent phase and composition control is mandatory to achieve high device efficiency. Very recently, lead iodide perovskite solar cells have attracted much attention because of its soaring device efficiency[6,7] and simple fabrication process. However, the toxicity of Pb and the stability issue cast some doubt on its further commercialization. Other potential absorber materials such as SnS,[8] Cu_2O,[9] Cu_2S,[10] and FeS_2[11,12] have been under study for years but the efficiencies are far away from expectation.

Sb_2Se_3 is a typical V_2−VI_3 binary chalcogenide with single phase and fixed composition,[13] avoiding the complexity of phase and defect control as in CZTSSe.[14] Sb_2Se_3 displays a narrow band gap of 1.1−1.3 eV,[15,16] which approaches the ideal Shockley−Queisser value.[17] Theoretical calculations demonstrated that Sb_2Se_3 is a promising candidate for achieving >20% device efficiency.[15,16] Furthermore, Sb and Se are abundant and low-toxicity materials, making Sb_2Se_3 very promising for photovoltaic application. So far most relevant work focused on the characterization of Sb_2Se_3 film produced from chemical bath deposition (CBD)[18,19] or electrodeposition.[20,21] The photovoltaic performance of Sb_2Se_3-based solar cell has rarely been demonstrated. Only until this year S. I. Seok's group presented Sb_2Se_3 sensitized inorganic−organic heterojunction solar cells and achieved an impressive device efficiency of 3.21%.[22] Sb_2Se_3 absorber was generated by thermal decomposition of Sb_2Se_3 single-source precursors into mesoporous TiO_2, and poly[2,6-(4,4-bis(2-ethylhexyl)-4*H*-cyclopenta[2,1-b;3,4-b′]-dithiophene)-*alt*-4,7-(2,1,3-benzothiadiazole)] (PCPDTBT) was selected as the hole-transporting material. R. Tena-Zaera's group reported a planar FTO/TiO_2/Sb_2Se_3/CuSCN/Au heterojunction device and obtained a device efficiency of 2.1%;[23] their Sb_2Se_3 was obtained from electrodeposition in an aqueous solution and CuSCN was applied as the hole conducting layer. At the same time, our group first reported a planar heterojunction FTO/TiO_2/Sb_2Se_3/Au device

Received: April 22, 2014
Accepted: June 12, 2014
Published: June 12, 2014

and achieved an encouraging solar conversion efficiency of 2.26% (V_{oc} = 0.52 V, J_{sc} = 10.3 mA/cm^2 and FF = 42.3%).[24] Hydrazine solution process was applied to build the Sb_2Se_3 absorber, and high V_{oc} and good device stability were demonstrated. The rapid efficiency progress achieved by multiple groups indicates that Sb_2Se_3 is indeed a very promising absorber material for solar cells.

Previous reports of Sb_2Se_3 solar cells exclusively relied on solution processing. Although these processes are possibly low-cost, they either employed toxic solvents and chemicals[22,24,25] or were prone to introducing contamination into the film.[23,26] Vacuum-based film deposition is simple and reliable, and has been successively applied in industrial manufacturing of CIGS[27] and CdTe[2] solar cells. Furthermore, Sb_2Se_3 has a low melting point[24] and high vapor pressure,[28] favoring easy thermal evaporation instead of magnetron sputtering.[29,30] Some groups applied thermally evaporated Sb_2Se_3 films as optical recording medium;[31−33] however, to the best of our knowledge, there is no report on Sb_2Se_3 thin-film solar cells using a vacuum-based process.

In this paper, we report the fabrication and characterization of thermally evaporated Sb_2Se_3 films, and their integration into a photovoltaic device with substrate configuration. Temperature-dependent vapor pressure of Sb_2Se_3 was first analyzed, followed by the systematic experimental study of the deposition conditions with special attention to the substrate temperature. Scanning electron microscopy (SEM), X-ray diffraction (XRD), Raman spectrum, X-ray photoemission spectrum (XPS), and photoresponse were applied to study the morphology, composition, and photosensitivity of as-deposited Sb_2Se_3 films. Finally, based on the ultraviolet photoelectron spectroscopy (UPS) derived band position, CdS was selected as the n-layer to build a planar photovoltaic device with substrate configuration of FTO/Sb_2Se_3/CdS/ZnO/ZnO:Al/Au and achieved 2.1% solar conversion efficiency.

2. EXPERIMENTAL SECTION

2.1. Deposition of Sb_2Se_3 Film. Sb_2Se_3 films were fabricated by thermal evaporation with 99.99% pure Sb_2Se_3 powder (Jiangxi Ketai Advanced Materials Co. Ltd.) using the electron beam and resistance evaporation thin film deposition system (Beijing Technol Science Co. Ltd.). FTO glass (5% haze) and Mo-coated soda-lime glass were used as substrates. Before deposition, substrate was subsequently cleaned in an ultrasonic bath using detergent, isopropanol and ethanol. The deposition chamber was pumped to a pressure of less than 5×10^{-4} Pa before evaporation. Excess Sb_2Se_3 powder was held in a quartz crucible (2 cc cylinder-shaped), which was twined with tungsten wire. The deposition rate was controlled by turning the current of tungsten filament, and monitored by microcrystalline quartz balance. The evaporation source was positioned 35 cm away from the sample holder (planar, 300 mm diameter). Deposition was carried out at different substrate temperatures (25, 150, 290 °C) to investigate the influence of substrate temperature to the properties of Sb_2Se_3 films and the performance of Sb_2Se_3 solar cells. Substrates were rear heated at an average rate of 10 °C/min from room temperature to the designed temperature. The evaporation source was preheated for 8 min before opening the shutter to deposit Sb_2Se_3 film. Deposition rate was kept at approximately 10 Å/s and lasted for 30 min. Continuous rotation of the sample holder with 3 rad/min during the deposition process facilitated the formation of homogeneous films. Afterward, the shutter was closed and the samples were cool down to room temperature naturally. Except for the 290 °C deposited sample, Sb_2Se_3 films deposited at 25 and 150 °C were further annealed at 290 °C for 10−20 min when the evaporation was closed to promote crystallization.

2.2. Photovoltaic Device Fabrication. 290 °Cdeposited Sb_2Se_3 film using FTO substrate was employed for device fabrication. Device architecture was substrate configuration FTO/Sb_2Se_3/CdS/ZnO/ZnO:Al/Au. CdS was grown by chemical bath deposition:[34] cadmium sulfate aqueous solution (0.015 M) and ammonium hydroxide aqueous solution (28%) were first mixed together with DI water and preheated for 1 min. Then thiourea aqueous solution was added, following by device loading. The whole solution was placed in a 65 °C water bath under continuous stirring for 16 min. The sample was further rinsed with DI water and dried under N_2 flow. Magnetron sputtered i-ZnO and ZnO:Al layers were grown after the deposition of CdS. The i-ZnO layer was deposited for 8 min with a power of 100 W, and the ZnO:Al layer was deposited for 40 min with a power of 300 W. Au electrode fingers with 100 μm width, 60 nm thickness and 1.3 mm spacing were deposited by thermal evaporation under vacuum pressure of 5×10^{-3} Pa. No antireflecting coating was used and the active area of our devices is 0.4 cm^2 defined by mechanical scribing.

2.3. Characterization and Measurements. The structure of Sb_2Se_3 film was investigated by X-ray diffraction (XRD) with Cu Kα radiation (Philips, X pert pro MRD). X-ray photoelectron spectroscopy (XPS) using Al Kα excitation (EDAX Inc. Genesis, 300W) and Raman spectrum (Horiba JobinYvon, LabRAM HR800, 532 nm excitation) were applied together to analyze the chemical nature of Sb_2Se_3. Thermogravimetric analysis (TGA, PerkinElmer Instruments, Diamond TG/DTA6300) was used to study the weight loss of Sb_2Se_3 powder at elevated temperatures. The test was carried out under N_2 flow, and the temperature was raised with a rate of 10 °C/min. Morphology of Sb_2Se_3 film was studied by SEM (FEI Nova NanoSEM450, without Pt coating). Photosensitivity of Sb_2Se_3 film was measured by Agilent (B1500A, America) inside an optically and electrically sealed box. Lighting was generated through a functional generator (Agilent 33210A) controlled 650 nm light-emitting diode which was biased at 5 V. UPS (Specs UVLS, He I excitation, 21.2 eV, referenced to the Femi edge of argon etched gold) was implemented to detect the Femi level and valence band of Sb_2Se_3 film. Thermoelectric effect measurement (The seebeck coefficient measuring instrument NI PXIe-1037) was carried out to study the conductivity type of Sb_2Se_3 films. Current−voltage measurements of Sb_2Se_3 solar cell were performed in a Newport Sol3A Class AAA Solar Simulator (450 W, Oriel, model 9119). Test was under an AM1.5 illumination to produce a 100 W/cm^2 solar irradiation at room temperature. The external quantum efficiency and reflection curves were measured using a Zolix SCS100 QE system equipped with a 150 W xenon light source, a lock-in amplifier, and an integrating sphere.

3. RESULTS AND DISCUSSION

3.1. Guidelines of Sb_2Se_3 Thermal Evaporation. Material properties of Sb_2Se_3 were first analyzed to gain insight for thermal evaporation. TGA analysis, run in N_2 with a ramp rate of 10 °C/min from room temperature to 800 °C, was employed to study the thermal stability of Sb_2Se_3 powder. Results are shown in Figure 1a. Weight loss started at approximately 423 °C,then sharply increased after 608 °C, which is the melting point of Sb_2Se_3 powder. Clearly, rapid evaporation would occur when Sb_2Se_3 power is heated up above 423 °C. This observation also suggested that the substrate temperature during evaporation should not exceed 423 °C; otherwise Sb_2Se_3 already deposited on the substrate would evaporate again and leave the substrate. This deduction was consistent with our experimental observation.

The evaporation details of Sb_2Se_3 were carefully studied by G.G. Gospodinov.[35] Their study suggested that Sb_2Se_3 could decompose during thermal evaporation following eq 1 in the temperature range of 677−822 K

$$Sb_2Se_3(s) = \frac{1}{4}Sb_4(g) + SbSe(g) + Se_2(g) \quad (1)$$

Obviously, congruent evaporation is not the case and presence of $Sb_4(g)$ and $Se_2(g)$ complicates the thermal evaporation

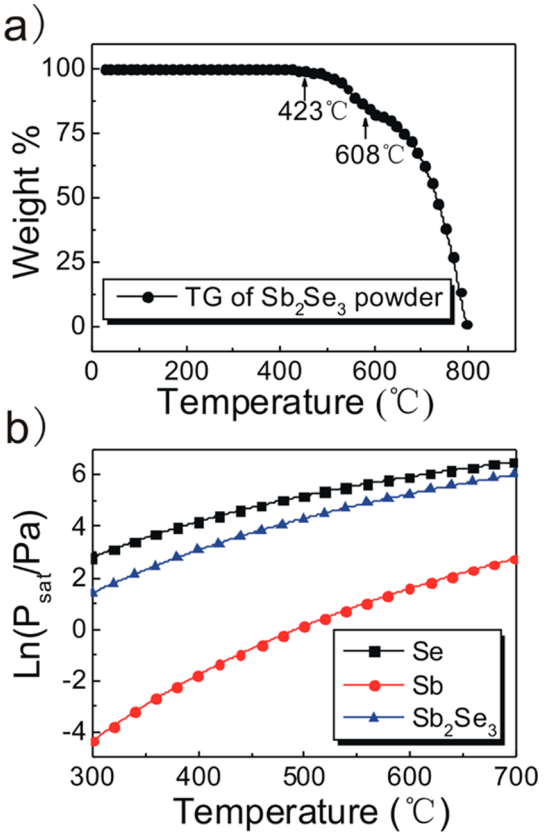

Figure 1. (a) Thermogravimetric analysis (TGA) of Sb_2Se_3 powder, which indicates the temperature of substrate should be lower than 423 °C during evaporation process. (b) Temperature-dependent saturated vapor pressure of Sb, Se, and Sb_2Se_3 in the temperature range from 300 to 700 °C.

process. To understand the Sb_2Se_3 evaporation better, we studied the temperature-dependent vapor-pressure of Sb_2Se_3, elemental Sb and elemental Se. Mathematical formulas relating the temperature and pressure of the gas phase in equilibrium with the condensed phase are listed below

$$\log p = A - \frac{B}{t + C} \quad (2)$$

$$\log p = A - \frac{B}{T} \quad (3)$$

In these equations, p is the vapor pressure of the compound in millimeter of mercury (mm Hg), t is the temperature in degree celsius, and T is the absolute temperature in kelvins (t °C +273.15). Equation 2 is the Antoine equation, which was used to calculate the pressure of Se. Equation 3 is applicable over restricted temperature ranges and was used to calculate vapor pressure of Sb and Sb_2Se_3.[28] Constants involved for calculation are shown in Table 1, and the temperature-dependent vapor–pressure equilibria for Sb_2Se_3, Sb, and Se are drawn in Figure 1b. First, Sb_2Se_3 has very high vapor pressure at elevated temperatures, 22.5 Pa at 400 °C and 3.48 × 10^3 Pa at 600 °C, confirming its easy evaporation stated before. Second, for all of the temperature range investigated, Se has a larger vapor pressure than Sb_2Se_3, and by far larger than Sb. The consequence of this difference will be discussed in detail later.

Table 1. Constants for Different Materials

substance	eq	A	B	C
Sb	2	9.051	9871	
Se	1	7.6316	4213	202
Sb_2Se_3	2	8.7906	6432.3	

3.2. Deposition and Characterization of Sb_2Se_3 Film.

Top-view and cross-sectional SEM imaging of Sb_2Se_3 films deposited at different temperatures (25, 150, and 290 °C) are shown in Figure 2. We defined the sample deposited at 25 °C and annealed at 290 °C as SS-25; sample deposited at 150 °C and annealed at 290 °C as SS-150; and sample deposited at 290 °C without further annealing as SS-290, respectively. For SS-25, both top-view SEM image (Figure 2a) and cross-sectional SEM image (Figure 2b) revealed the film was composed of large Sb_2Se_3 grains free of pinholes and cracks. Films was amorphous when deposited at 25 °C substrate temperature, and crystallized into large grains during the 290 °C annealing. Such a low crystallization temperature is a consequence of the low melting point of Sb_2Se_3, one advantage of Sb_2Se_3 for photovoltaic application. SS-290 also showed compact film with large grains (Figure 2e, f). The distinct difference between SS-25 and SS-290 is the surface roughness, the surface of SS-290 being dominated by rodlike Sb_2Se_3 with irregular shape and orientation. Sb_2Se_3 is intrinsically one-dimensional material and Sb_2Se_3 nanoneedles and nanorods were routinely observed from various synthetic methods.[36,37] Such a rough surface is not favorable for the construction of thin film solar cells. One additional difference between SS-25 and SS-290 was the adhesion between Sb_2Se_3 film and the FTO substrates. Abundant voids were observed at the interface between Sb_2Se_3 film and FTO substrate in sample SS-25, while the interface in sample SS-290 was compact and void-free, which is probably originated from the higher energy and better diffusion

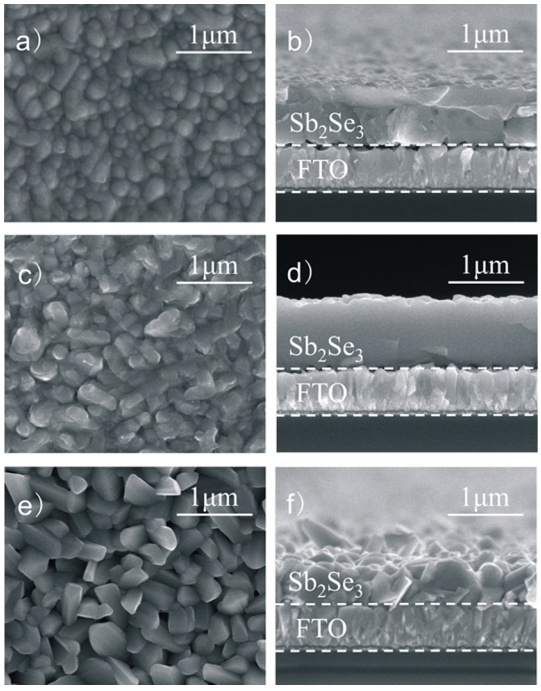

Figure 2. SEM of evaporated Sb_2Se_3 onto FTO. (a, b) Top-view and cross-sectional SEM of sample SS-25. (c, d) Top-view and cross-sectional SEM of sample SS-150. (e, f) Top-view and cross-sectional SEM of sample SS-290.

of Sb_2Se_3 species when deposited onto 290 °C substrate. Sample SS-150, shown in Figure 2c, d, was transitional between SS-25 and SS-290 and hence has medium surface roughness and interfacial voids. It should be mentioned that we also tried deposition of Sb_2Se_3 film onto Mo coated soda-lime glass, the standard substrate for CIGS solar cells. However, the film peeled off during the ZnO and ZnO:Al sputtering process employed for device fabrication. During our Sb_2Se_3 deposition, the maximum substrate temperature was 290 °C, thus the formation of $MoSe_2$ between Mo and Sb_2Se_3 is very limited, possibly accounting for the poor adhesion between thermally evaporated Sb_2Se_3 and Mo substrates.[38]

X-ray diffraction (XRD) was applied to characterize Sb_2Se_3 films deposited at different temperatures. As shown in Figure 3a, taking no account of diffraction peaks of FTO, the diffraction peaks of our samples (SS-25, SS-150 and SS-290) agreed very well with orthorhombic Sb_2Se_3 (JCPDS 15−0861). Major peaks were indexed to the diffraction planes and no secondary phase or impurity was detected. Films deposited at lower temperature (SS-25 and SS-150) showed preferred orientation along the [020] and [120] direction, whereas SS-290 showed no preferred orientation. The influence of thermal processing on Sb_2Se_3 film orientation is under study to reveal the underlying mechanism.

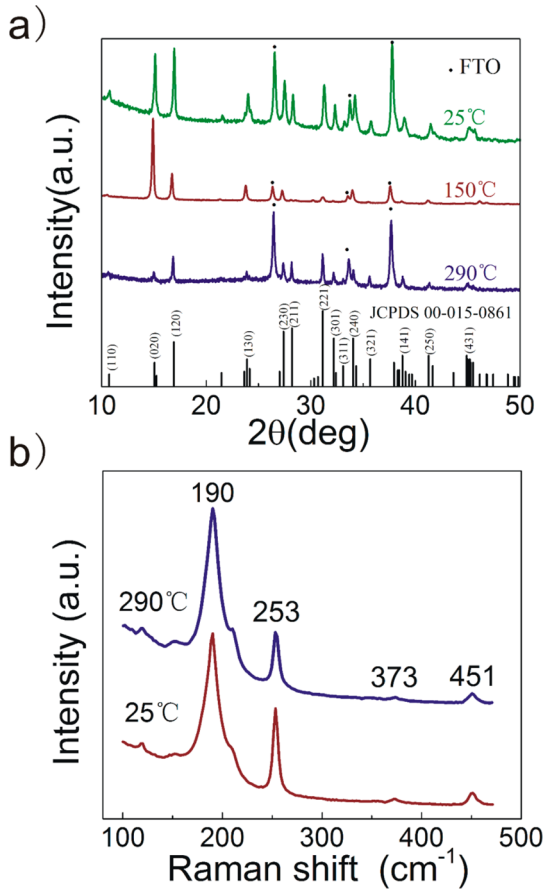

Figure 3. (a) X-ray diffraction patterns of Sb_2Se_3 films on FTO at different deposition temperature. Films deposited at different temperature (SS-25, SS-150, and SS-290) have different orientation. (b) Raman spectra of Sb_2Se_3 films (SS-25 and SS-290). Peaks centered at 190 and 253 cm^{-1} belong to Sb_2Se_3, and peaks at 373 and 451 cm^{-1} belong to Sb_2O_3.

Raman spectra of Sb_2Se_3 films (SS-25 and SS-290) were performed at room temperature with a 532 nm laser as excitation source. The results are shown in Figure 3b. For both samples, two Raman bands centered at 190 and 253 cm^{-1} were observed, representing the heteropolar Sb−Se and Sb−Sb nonpolar vibrations, respectively, which are characteristic of Sb_2Se_3.[39] There were two more Raman bands centered at 373 and 451 cm^{-1}, which are characteristic of Sb_2O_3.[40] No difference in Raman spectra was observed for Sb_2Se_3 deposited at 25 and 290 °C.

X-ray photoelectron spectroscopy (XPS) measurements were further carried out to study the chemistry state of Sb_2Se_3 as well as the presence of Sb_2O_3. Sb_2Se_3 films (SS-25 and SS-290) were kept strictly inside a N_2 atmosphere with a brief air exposure (~10 min for sample preparation and loading) before XPS measurement. Because SS-25 and SS-290 showed identical XPS results, we thus limit our discussion to SS-290 here. For clarity, binding energies of Sb 4d, Sb 3d, Se 3d, and O 1s are shown in Table 2. Panels a, c, and d in Figure 4 show magnified XPS spectra of Sb 3d, Sb 4d, and Se 4d of Sb_2Se_3 film. An oxygen peak was observed in Figure 4a, and its binding energy of 532.91 eV suggested the existence of Sb_2O_3,[41,42] which was in accord with Raman results. Because XPS is a surface sensitive technique, we etched the sample by Ar^+ ion sputtering for 600 s (~10 nm thickness) and repeated XPS measurement. Peak of O 1s disappeared as shown in Figure 4b, indicating Sb_2O_3 only presented on the top surface of Sb_2Se_3 film. All Sb 4d and Se 4d peaks (in both fresh and etched samples) could be perfectly

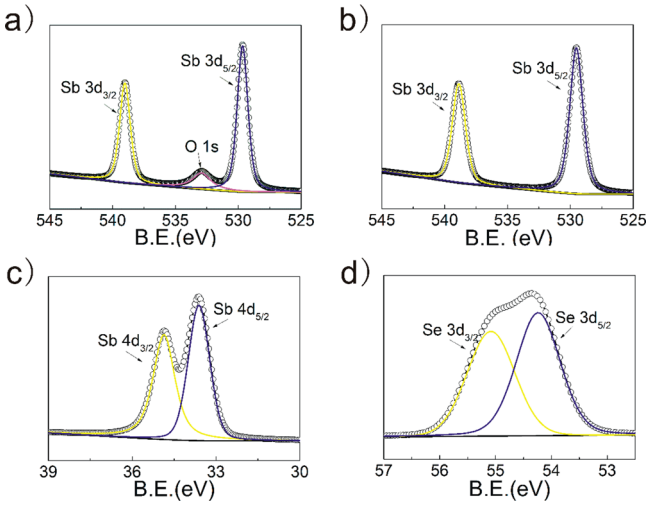

Figure 4. XPS spectra of Sb_2Se_3 film. (a, c, d) Magnified XPS spectra of fresh Sb_2Se_3 film. (b) Magnified XPS spectra of Sb 3d in the plasma-etched Sb_2Se_3 film.

Table 2. Binding Energy of Different Elements

condition	Sb $4d_{5/2}$	Sb $4d_{3/2}$	Sb $3d_{5/2}$	Sb $3d_{3/2}$	Se $3d_{5/2}$	Se $3d_{3/2}$	O 1s
fresh	33.6	34.85	529.65	539.02	54.23	55.07	532.91
etched for 600 s			529.92	538.87			

fitted with Gaussian−Lorentzian peaks, and their binding energies were in good agreement with the expected value in Sb_2Se_3,[43] excluding the presence of Sb^{5+} or elemental Se in our sample. In other words, the bulk of our sample was pure Sb_2Se_3 with some Sb_2O_3 presented on the surface.

We now discuss the origin of Sb_2O_3 in our sample. First, it is not likely that Sb_2O_3 was formed by oxidizing Sb_2Se_3 during sample preparation. When Sb_2Se_3 is oxidized into Sb_2O_3, Se is the most likely side-product but we failed to detect pure Se from XPS measurement. Furthermore, we also followed the same procedure to measure XPS spectrum of hydrazine processed Sb_2Se_3 film but observed no oxygen peak.[24] We tentatively proposed that oxidization of Sb impurities in Sb_2Se_3 film during sample preparation accounted for the presence of Sb_2O_3. Because of its very low vapor pressure (Figure 1b), Sb species reside in the evaporator chamber (formed during thermal evaporation) would condense onto Sb_2Se_3 film surface during the cooling process easily. Once exposed to air, Sb would immediately react with O_2 forming Sb_2O_3 due to the large Gibbs free energy (−605 kJ/mol) and standard molar reaction enthalpy (−718 kJ/mol). The reaction between Sb with Se is more difficult than with O_2 because of the small Gibbs free energy (−125 kJ/mol) and standard molar reaction enthalpy (−128 kJ/mol).[44]

3.3. Optical Property, Photosensitivity, and Band Position of Sb_2Se_3 Film. It should be noted that Sb_2Se_3 film deposited onto FTO with low substrate temperatures (25 and 150 °C) all fell off when sputter ZnO and ZnO:Al during photovoltaic device preparation, which is probably due to the voids presented at the interface between Sb_2Se_3 film and FTO substrates (Figure 2a−d). Resolving the adhesion problem is beyond the scope of this paper, and we thus limit our following discussion to Sb_2Se_3 film thermally evaporated onto 290 °C FTO substrates.

We first applied transmittance measurement to determine the optical transition type (direct or indirect) and band gap of Sb_2Se_3 film deposited at 290 °C. PerkinElmer Instuments (Lambda 950) equipped with an integrating sphere was applied for the measurement and the results are included in Figure 5. Beginning at ∼1050 nm, film transmittance reduced steeply and decreased to almost zero at wavelength shorter than 900 nm. Using the film thickness determined by cross-sectional SEM imaging, the absorption coefficient α of Sb_2Se_3 film deposited at 290 °C was obtained and shown in Figure 5b. The absorption coefficient increased rapidly at ∼1.2 eV, and reached 6×10^4 cm^{-1} for approximately 1.4 eV photons. The slow increase in absorption coefficient between 1.1 to 1.2 eV may suggest a possible indirect band gap. Nonetheless, we observed nice linear zone by plotting $(\alpha h\nu)^2$ versus $(h\nu)$ and obtained an optical band gap of 1.2 eV by extrapolating the linear portion of the plot to its x-intercept. The value was slightly larger than the value from literature[45] and our previous report.[24]

Photosensitivity of Sb_2Se_3 films was investigated by evaporating Au electrodes onto sample SS-290 to build a photodetector. Device area was determined by the electrode length (3 mm) and interelectrodes spacing (0.2 mm). Testing was done inside an optically and electrically sealed box, and lighting (650 nm wavelength, 430 $\mu W/cm^2$) was generated through a functional generator controlled light-emitting diode. Au contact was measured to be ohmic, so our device is a photoconductive photodetector. As shown in Figure 6a, strong and reversible photoresponse was observed. When biased at 40 V, this device showed a dark current of 9 nA, a photocurrent of

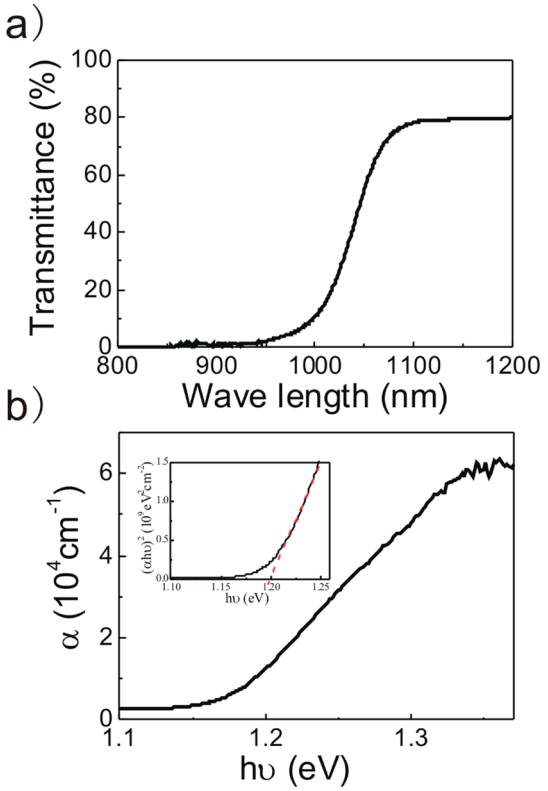

Figure 5. (a) Transmission spectra of Sb_2Se_3 film on FTO. (b) Absorption coefficient of Sb_2Se_3 film. Insert, tauc plot (n = 2; direct) for Sb_2Se_3 film (E_g = 1.2 eV).

61 nA, corresponding to an phototo-dark current ratio of 7. Because the Hall Effect measurement failed on our thermal evaporated Sb_2Se_3 film, we estimated the doping density of Sb_2Se_3 film using the conductivity data from the photodetector measurement. Assuming the same mobility for the evaporated and hydrazine processed Sb_2Se_3 film (5.1 $cm^2/(V\ s)$, from Hall effect measurement), we obtained a doping (hole) density of approximately 5.3×10^{12} cm^{-3} for our evaporated Sb_2Se_3 film. We also constructed a photodetector with identical device configuration using hydrazine solution processed Sb_2Se_3 film, and the device performance was shown in Figure S1 in the Supporting Information. Clearly, the hydrazine-derived Sb_2Se_3 device showed much smaller and more sluggish photoresponse, suggesting our vacuum-based Sb_2Se_3 is of higher quality. By measuring the transient photocurrent decay, the lifetime of trapped carriers could be further estimated by fitting the tail of the decay curves with two exponential functions and expresses by the formula

$$y = y_0 + A_1 e^{-(x-x_0)/t_1} + A_2 e^{-(x-x_0)/t_2} \quad (4)$$

The fitting yielded two time constants of 0.16 and 2.8 ms. In photoconductive photodetector, photocurrent decay kinetics strongly correlates to the trap depths; shallow traps result in fast photoresponse.[46] Considering 60 ms photoresponse corresponds to 0.09 eV trap depth below the conduction band in PbS colloidal quantum dot photoconductive photodetectors,[47,48] much shallower trap depth would be expected in our SS-290 film. Strong photoresponse and possible low trap depth suggest good optoelectronic properties of Sb_2Se_3 film deposited at 290 °C.

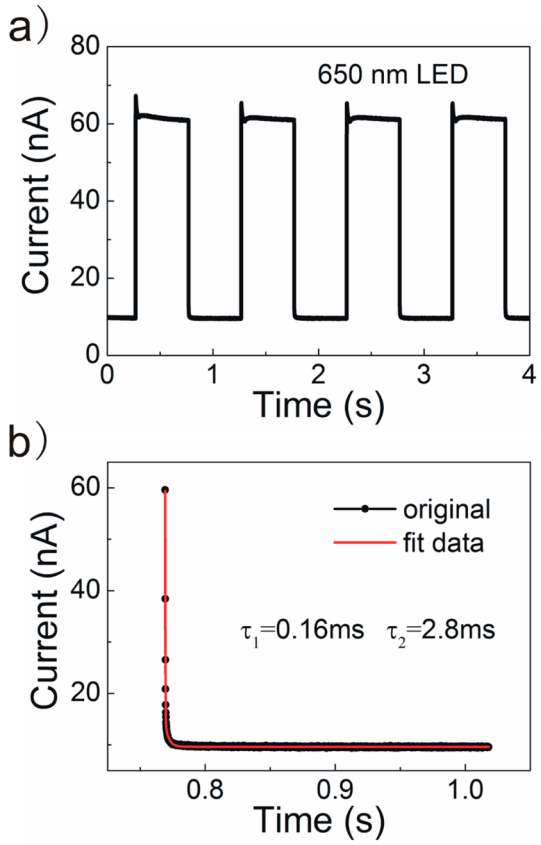

Figure 6. (a) Photosensitivity of Sb_2Se_3 film deposited at 290 °C (SS-290) on glass. Sb_2Se_3 film was illuminated under 650 nm LED, whose power density is 430 $\mu W/cm^2$. Current was tested using 40 V driving voltage. (b) Fitting curve of photocurrent decay. Two exponential decay components with time constants of 0.16 ms and 2.8 ms were obtained.

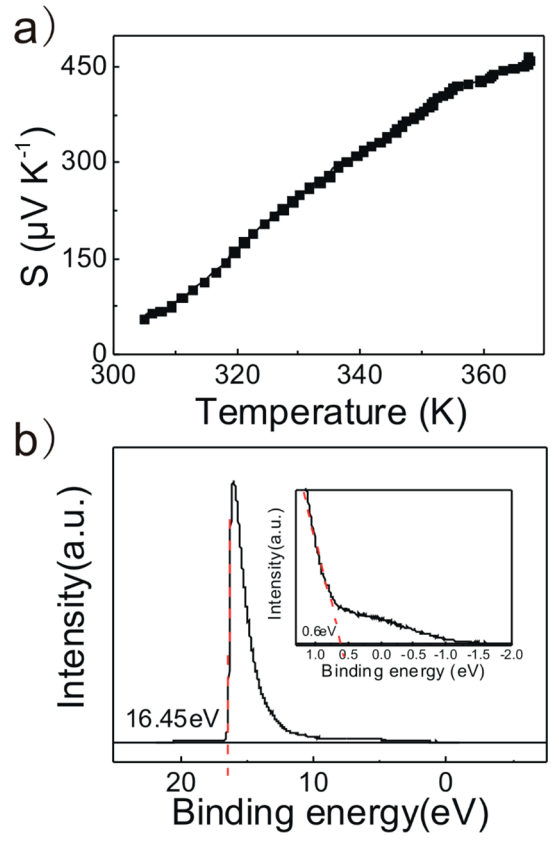

Figure 7. (a) Temperature dependence of the Seebeck coefficient of the Sb_2Se_3 film. (b) UPS spectrum of Sb_2Se_3 film. Inset plot is the fitting of the long-tail spectrum.

Thermoelectric effect measurement was implemented to study the conductivity type of Sb_2Se_3 films. As shown in Figure 7a, positive Seebeck coefficient confirmed that our Sb_2Se_3 is a p-type semiconductor. We also applied ultraviolet photoelectron spectroscopy to measure the band position of SS-290 film (Figure 7b). Au was thermally evaporated onto SS-290 film for calibration. Fermi energy was first obtained as −4.75 eV by subtracting the spectrum onset of 16.45 eV with the ultraviolet photon energy of 21.2 eV. The distance between the valence band miximum (VBM) and the Fermi energy was calculated as 0.60 eV (by fitting the long-tail spectrum insert in Figure 7). We thus conclude that VBM and conduction band maximum (CBM) of our Sb_2Se_3 locates at −5.35 and −4.15 eV, respectively. For comparison, we also applied UPS to measure the hydrazine processed Sb_2Se_3 film and obtained the same VBM position of −5.35 eV. This value, however, is different from the previous results derived from cyclic voltammetry measurement (−3.90 eV and −4.92 eV).[24] Because UPS is a more reliable tool to characterize band position, we believe that the VBM of Sb_2Se_3 should be at −5.35 eV.

3.4. Solar Cell Fabrication and Performance. Substrate (CIGS type) and superstrate (CdTe type) configurations are all possible for Sb_2Se_3 solar cell. In this article, substrate structure FTO/Sb_2Se_3/CdS/ZnO/ZnO:Al/Au (Figure 8a) was chosen to make Sb_2Se_3 solar cells, and illumination was from the gap between Au fingers at top. FTO instead of Mo covered glass was selected as the substrate because of poor adhesion of SS-290 film to Mo as stated previously. The band diagram between Sb_2Se_3 and CdS was drawn in Figure 8b. Band position and Fermi energy value for chemical bath deposited CdS layer is adopted from literature.[49] Clearly, band alignment between Sb_2Se_3 and CdS favors photogenerated electrons flowing from Sb_2Se_3 to CdS, and the large VBM offset blocks holes injection into CdS. It should be noted that this band diagram was approximated from sketchy band information and future experimental verification is required. Figure 8c shows current

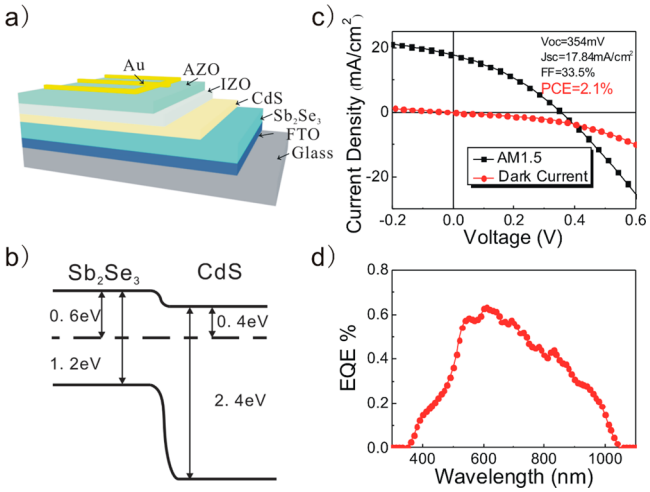

Figure 8. (a) Schematic demonstration of the device configuration, (b) sketchy band diagram, (c) dark and light current density curves, and (d) EQE spectrum of Sb_2Se_3 solar cell.

density−voltage characteristics of our best Sb_2Se_3 solar cells under 100 mW/cm^2 simulated AM1.5G irradiation. The champion device exhibited a short-circuit current density (J_{sc}) of 17.8 mA/cm^2, an open circuit voltage (V_{oc}) of 0.354 V, and a fill factor (FF) of 33.5%, corresponding to a solar to electricity conversation efficiency (η) of 2.1%. If the light illumination was from the FTO side, Jsc would decrease to 10 mA/cm^2. When illuminated from the FTO side, most of incident photons were absorbed by the Sb_2Se_3 film near FTO substrate. These photogenerated electrons (minority carriers) have to travel through the whole Sb_2Se_3 film to reach the Sb_2Se_3/CdS heterojunction interface and get separated. Not surprisingly, severe recombination loss would occur during this traipse, leading to substantially reduced J_{sc}. To compare the quality between thermally evaporated and hydrazine-processed Sb_2Se_3 films, we further built FTO/Sb_2Se_3/CdS/ZnO/ZnO:Al/Au solar cells using hydrazine solution-processed Sb_2Se_3 film. Typical devices showed V_{oc} of 0.31 V, J_{sc} of 14.5 mA/cm^2, FF of 33.3%, and efficiency of 1.47%. The slightly lower J_{sc} in hydrazine processed Sb_2Se_3 solar cells was probably due to its severe recombination loss, as evidenced by the smaller and more sluggish photoresponse observed in hydrazine processed Sb_2Se_3 photoconductive photodetectors. We thus conclude that the quality of thermally evaporated Sb_2Se_3 films was better than hydrazine-processed Sb_2Se_3 films. However, this conclusion is tentative considering very limited optimization work done so far on the FTO/Sb_2Se_3/CdS/ZnO/ZnO:Al/Au solar cells using hydrazine-processed Sb_2Se_3 films.

The external quantum efficiency (EQE) spectrum of this 2.1% efficient Sb_2Se_3 solar cell is presented in Figure 8d. EQE spectrum started from 1050 nm, which was consistent with the transmittance measurement. The EQE spectrum reached a maximum value of 0.6 at ∼600 nm, then declined both in the shorter and longer wavelength due to the strong CdS absorption and the insufficient generation and collection of carriers at the back side (i.e., zones close to the FTO contact), respectively. Compared with the >90% plateau of EQE spectrum observed in highly efficient CIGS solar cells,[27] our Sb_2Se_3 solar cells have much room for improvement. Possible directions include increasing carrier mobility and lifetime through Sb_2Se_3 film optimization, and substitution of CdS with other buffer layer like ZnS and Zn(O,S).

In our Sb_2Se_3 solar cell, the V_{oc} is 354 mV, which is larger than previous Sb_2Se_3 sensitized (V_{oc} = 304.5 mV)[22] and electrodeposited Sb_2Se_3 (V_{oc} = 302 mV) solar cells. This value, however, is much smaller than our own Sb_2Se_3/TiO_2 solar cells made by solution-processing (V_{oc} = 520 mV).[24] Doping concentration of TiO_2 made by sol−gel process (∼1 × 10^{15} cm^{-3}) is lower than that of CdS made by chemical bath deposition (∼1 × 10^{17} cm^{-3}). Cleary, the V_{oc} loss in our solar cells is not originated from the CdS doping, but from many other aspects. One obvious reason was the very rough surface of our thermally evaporated Sb_2Se_3 film, which severely increased the heterojunction area and hence the reverse saturation current, as evidenced by the poor rectification of the dark current shown in Figure 8c. Other possibilities include the improper band alignment or harmful interfacial reaction between Sb_2Se_3 and CdS, the low doping density and high defect density of Sb_2Se_3 film, as well as contact problems. Our solar cell is also limited by the very low FF of 33.5%, which is most likely due to the poor Sb_2Se_3/CdS junction and the less optimized sputtering process of ZnO and ZnO:Al as the shunt resistance (131.4 ohm) is low and the series resistance (29.8 ohm) is high. For sure, there is much work to do to optimize device configuration and materials processing. Nonetheless, the 2.1% device efficiency is very encouraging for this thermally evaporated Sb_2Se_3 solar cell.

4. CONCLUSION

In summary, we presented Sb_2Se_3 heterojunction solar cells made from thermal evaporation. A prototype substrate FTO/Sb_2Se_3/CdS/ZnO/ZnO:Al/Au solar cell was built and 2.1% device efficiency (V_{oc} = 354 mV, J_{sc} = 17.84 mA/cm^2, FF = 33.5%) was obtained under simulated AM1.5G irradiation. Major findings associated with thermally evaporated Sb_2Se_3 film include: (i) large-grain, crack-, and pinhole-free Sb_2Se_3 film can be directly obtained by thermal evaporation at low substrate temperatures (up to 290 °C); (ii) as-prepared Sb_2Se_3 film is p-type with extremely low doping density and has a band gap of 1.2 eV with VBM and CBM located at −5.35 and −4.15 eV, respectively; (iii) adhesion is a major problem associated with thermally evaporated Sb_2Se_3 film, limiting substrate choice and deposition temperature; (iv) Sb and Sb_2O_3 (once exposed to air) contamination could occur in Sb_2Se_3 film because of the decomposition of Sb_2Se_3 during thermal evaporation. Our findings suggest that thermal evaporation is a viable and competitive strategy to produce Sb_2Se_3 films and photovoltaic devices. Further material understanding and process optimization should be done to improve the device efficiency of these very promising Sb_2Se_3 solar cells.

■ ASSOCIATED CONTENT

Supporting Information

Photoresponse of solution-processed Sb_2Se_3 film, performance of solution-processed Sb_2Se_3 solar cells with the architecture FTO/Sb_2Se_3/CdS/ZnO/ZnO:Al/Au. This material is available free of charge via the Internet at http://pubs.acs.org.

■ AUTHOR INFORMATION

Corresponding Author

*E-mail: jtang@mail.hust.edu.cn.

Author Contributions

[§]X.L. and J.C. contributed equally to this manuscript. All authors commented on and approved the final version of this manuscript.

Notes

The authors declare no competing financial interest.

■ ACKNOWLEDGMENTS

Prof. Daocheng Pan and Dr. Gang Wang are acknowledged for their help in ZnO and ZnO:Al sputtering and EQE measurement help. Yuchun Liu is acknowledged for her help to conduct the thermoelectric effect measurement. This work is financially supported by the seed project of Wuhan National Latboratory for Optoelectronics, the "National 1000 Young Talents" project, National Natural Science Foundation of China (NSFC 61274055, 61322401), China Postdoctoral Science Foundation (2013M542015), and Fundamental Research Funds for the Central Universities, HUST (0118187043, CXY12M008). The Analytical and Testing Center of HUST and the Center for Nanoscale Characterization and Devices of WNLO are also acknowledged for the characterization support. The authors also thank Beijing Technol Sciences Co. Ltd for thermal evaporation technical assistance.

REFERENCES

(1) Green, M. A.; Emery, K.; Hishikawa, Y.; Warta, W.; Dunlop, E. D. Solar Cell Efficiency Tables (Version 43). *Prog. Photovolt.: Res. Appl.* **2014**, *22*, 1.

(2) Fist Solar Sets World Record for CdTe Solar Cell Efficiency. http://investor.firstsolar.com/releasedetail.cfm?ReleaseID=828273 (accessed Mar 8, 2014).

(3) Wang, W.; Winkler, M. T.; Gunawan, O.; Gokmen, T.; Todorov, T. K.; Zhu, Y.; Mitzi, D. B. Device Characteristics of CZTSSe Thin-Film Solar Cells with 12.6% Efficiency. *Adv. Energy Mater.* **2013**, DOI: 10.1002/aenm.201301465.

(4) Wang, G.; Wang, S.; Cui, Y.; Pan, D. A Novel and Versatile Strategy to Prepare Metal-Organic Molecular Precursor Solutions and Its Application in $Cu(In,Ga)(S,Se)_2$ Solar Cells. *Chem. Mater.* **2012**, *24*, 3993.

(5) Wang, G.; Zhao, W.; Cui, Y.; Tian, Q.; Gao, S.; Huang, L.; Pan, D. Fabrication of a $Cu_2ZnSn(S,Se)_4$ Photovoltaic Device by a Low-Toxicity Ethanol Solution Process. *ACS Appl. Mater. Interfaces* **2013**, *5*, 10042.

(6) Burschka, J.; Pellet, N.; Moon, S.-J.; Humphry-Baker, R.; Gao, P.; Nazeeruddin, M. K.; Grätzel, M. Sequential Deposition as a Route to High-Performance Perovskite-Sensitized Solar Cells. *Nature* **2013**, *499*, 316.

(7) Liu, M.; Johnston, M. B.; Snaith, H. J. Efficient Planar Heterojunction Perovskite Solar Cells by Vapour Deposition. *Nature* **2013**, *501*, 395.

(8) Sinsermsuksakul, P.; Hartman, K.; Bok Kim, S.; Heo, J.; Sun, L.; Hejin Park, H.; Chakraborty, R.; Buonassisi, T.; Gordon, R. G. Enhancing the Efficiency of SnS Solar Cells via Band-Offset Engineering with a Zinc Oxysulfide Buffer Layer. *Appl. Phys. Lett.* **2013**, *102*, 053901.

(9) Mittiga, A.; Salza, E.; Sarto, F.; Tucci, M.; Vasanthi, R. Heterojunction Solar Cell with 2% Efficiency Based on a Cu_2O Substrate. *Appl. Phys. Lett.* **2006**, *88*, 163502.

(10) Wu, Y.; Wadia, C.; Ma, W.; Sadtler, B.; Alivisatos, A. P. Synthesis and Photovoltaic Application of Copper (I) Sulfide Nanocrystals. *Nano Lett.* **2008**, *8*, 2551.

(11) Puthussery, J.; Seefeld, S.; Berry, N.; Gibbs, M.; Law, M. Colloidal Iron Pyrite (FeS_2) Nanocrystal Inks for Thin-Film Photovoltaics. *J. Am. Chem. Soc.* **2010**, *133*, 716.

(12) Berry, N.; Cheng, M.; Perkins, C. L.; Limpinsel, M.; Hemminger, J. C.; Law, M. Atmospheric-Pressure Chemical Vapor Deposition of Iron Pyrite Thin Films. *Adv. Energy Mater.* **2012**, *2*, 1124.

(13) Ghosh, G. The Sb-Se (Antimony-Selenium) System. *J. Phase Equilib.* **1993**, *14*, 753.

(14) Xu, P.; Chen, S.; Huang, B.; Xiang, H.-J.; Gong, X.-G.; Wei, S.-H. Stability and Electronic Structure of Cu_2ZnSnS_4 Surfaces: First-Principles Study. *Phys. Rev. B* **2013**, *88*, 045427.

(15) Patrick, C. E.; Giustino, F. Structural and Electronic Properties of Semiconductor-Sensitized Solar-Cell Interfaces. *Adv. Funct. Mater.* **2011**, *21*, 4663.

(16) Filip, M. R.; Patrick, C. E.; Giustino, F. GW Quasiparticle Band Structures of Stibnite, Antimonselite, Bismuthinite, and Guanajuatite. *Phys. Rev. B* **2013**, *87*, 205125.

(17) Shockley, W.; Queisser, H. J. Detailed Balance Limit of Efficiency of P-N Junction Solar Cells. *J. Appl. Phys.* **1961**, *32*, 510.

(18) Maghraoui-Meherzi, H.; Ben Nasr, T.; Dachraoui, M. Synthesis, Structure and Optical Properties of Sb_2Se_3. *Mater. Sci. Semicond. Process.* **2013**, *16*, 179.

(19) Rodríguez-Lazcano, Y.; Peña, Y.; Nair, M. T. S.; Nair, P. K. Polycrystalline Thin Films of Antimony Selenide via Chemical Bath Deposition and Post Deposition Treatments. *Thin Solid Films* **2005**, *493*, 77.

(20) Lai, Y.; Chen, Z.; Han, C.; Jiang, L.; Liu, F.; Li, J.; Liu, Y. Preparation and Characterization of Sb_2Se_3 Thin Films by Electrodeposition and Annealing Treatment. *Appl. Surf. Sci.* **2012**, *261*, 510.

(21) Shi, X.; zhang, X.; Tian, Y.; Shen, C.; Wang, C.; Gao, H.-J. Electrodeposition of Sb_2Se_3 on Indium-Doped Tin Oxides Substrate: Nucleation and Growth. *Appl. Surf. Sci.* **2012**, *258*, 2169.

(22) Choi, Y. C.; Mandal, T. N.; Yang, W. S.; Lee, Y. H.; Im, S. H.; Noh, J. H.; Seok, S. I. Sb2Se3-sensitized Inorganic-Organic Heterojunction Solar Cells Fabricated Using a Single-Source Precursor. *Angew. Chem., Int. Ed.* **2014**, *53*, 1329.

(23) Ngo, T. T.; Chavhan, S.; Kosta, I.; Miguel, O.; Grande, H. J.; Tena-Zaera, R. Electrodeposition of Antimony Selenide Thin Films and Application in Semiconductor Sensitized Solar Cells. *ACS Appl. Mater. Interfaces* **2014**, *6*, 2836.

(24) Zhou, Y.; Leng, M.; Xia, Z.; Zhong, J.; Song, H.; Liu, X.; Yang, B.; Zhang, J.; Chen, J.; Zhou, K.; Han, J.; Cheng, Y.; Tang, J. Solution-Processed Antimony Selenide Heterojunction Solar Cells. *Adv. Energy Mater.* **2014**, DOI: 10.1002/aenm.201301846.

(25) Choi, Y. C.; Lee, Y. H.; Im, S. H.; Noh, J. H.; Mandal, T. N.; Yang, W. S.; Seok, S. I. Efficient Inorganic-Organic Heterojunction Solar Cells Employing $Sb_2(S_x/Se_{1-x})_3$ Graded-Composition Sensitizers. *Adv. Energy Mater.* **2014**, DOI: 10.1002/aenm.201301680.

(26) Calixto-Rodriguez, M.; García, H. M.; Nair, M.; Nair, P. Antimony Chalcogenide/Lead Selenide Thin Film Solar Cell with 2.5% Conversion Efficiency Prepared by Chemical Deposition. *ECS J. Solid State Sci. Technol.* **2013**, *2*, Q69.

(27) Jackson, P.; Hariskos, D.; Lotter, E.; Paetel, S.; Wuerz, R.; Menner, R.; Wischmann, W.; Powalla, M. New World Record Efficiency for $Cu(In,Ga)Se_2$ Thin-Film Solar Cells Beyond 20%. *Prog. Photovolt.: Res. Appl.* **2011**, *19*, 894.

(28) Speight, J. G. *Lange's Handbook of Chemistry*; McGraw-Hill: New York, 2005; Vol. *1*, pp 199−219.

(29) Carcia, P.; McLean, R.; Reilly, M.; Nunes, G. Transparent ZnO Thin-Film Transistor Fabricated by RF Magnetron Sputtering. *Appl. Phys. Lett.* **2003**, *82*, 1117.

(30) Tanemura, S.; Miao, L.; Jin, P.; Kaneko, K.; Terai, A.; Nabatova-Gabain, N. Optical Properties of Polycrystalline and Epitaxial Anatase and Rutile TiO_2 Thin Films by RF Magnetron Sputtering. *Appl. Surf. Sci.* **2003**, *212*, 654.

(31) Harea, D.; Iovu, M.; Iaseniuc, O.; Colomeico, E.; Meshalkin, A.; Iovu, M. Modification of the Optical Constants in Amorphous Sb_2Se_3: Sn Thin Films under the Illumination and Heat Treatment. *J. Optoelectron. Adv. Mater.* **2009**, *11*, 2039.

(32) Kaito, C.; Fujita, T.; Kimura, T.; Hanamoto, K.; Suzuki, N.; Kimura, S.; Saito, Y. Structure and Crystallization of SbSe Films Prepared by Vacuum Evaporation Method. *Thin Solid Films* **1998**, *312*, 93.

(33) songsheng, Xue; Z, F.; Fuxi, Gan Optical Properities and Microstructure of Phase Change Recording Media Sb_2Se_3 Thin Films. *Chin. J. Lasers* **2000**, *10*, 77.

(34) Contreras, M. A.; Romero, M. J.; To, B.; Hasoon, F.; Noufi, R.; Ward, S.; Ramanathan, K. Optimization of CBD CdS Process in High-Efficiency $Cu(In,Ga)Se_2$-based solar cells. *Thin Solid Films* **2002**, *403*, 204.

(35) Gospodinov, G.; Pashinkin, A.; Boncheva-Mladenova, Z.; Novoselova, A. Determination of the Saturated Vapour Pressure of Solid Antimony Selenide. *Izv. Akad. Nauk Est. SSR, Fiz. Mater.* **1970**, *6*, 726.

(36) Wang, J.; Deng, Z.; Li, Y. Synthesis and Characterization of Sb_2Se_3 Nanorods. *Mater. Res. Bull.* **2002**, *37*, 495.

(37) Ma, J.; Wang, Y.; Wang, Y.; Peng, P.; Lian, J.; Duan, X.; Liu, Z.; Liu, X.; Chen, Q.; Kim, T. One-Dimensional Sb_2Se_3 Nanostructures: Solvothermal Synthesis, Growth Mechanism, Optical and Electrochemical Properties. *CrystEngComm* **2011**, *13*, 2369.

(38) Abou-Ras, D.; Kostorz, G.; Bremaud, D.; Kälin, M.; Kurdesau, F. V.; Tiwari, A. N.; Döbeli, M. Formation and Characterisation of $MoSe_2$ for $Cu(In,Ga)Se_2$ Based Solar Cells. *Thin Solid Films* **2005**, *480−481*, 433.

(39) Liu, Y.-Q.; Zhang, M.; Wang, F.-X.; Pan, G.-B. Facile Microwave-Assisted Synthesis of Uniform Sb_2Se_3 Nanowires for High Performance Photodetectors. *J. Mater. Chem. C* **2014**, *2*, 240.

(40) Cebriano, T.; Méndez, B.; Piqueras, J. Micro- and Nanostructures of Sb_2O_3 Grown by Evaporation–Deposition: Self Assembly Phenomena, Fractal and Dendritic Growth. *Mater. Chem. Phys.* **2012**, *135*, 1096.
(41) Paparazzo E. *NIST X-ray Photoelectron Spectroscopy Database*. http://srdata.nist.gov/xps/EngElmSrchQuery.aspx?EType=PE&CSOpt=Retri_ex_dat&Elm=O (accessed Feb 25, 2014).
(42) Honma, T.; Sato, R.; Benino, Y.; Komatsu, T.; Dimitrov, V. Electronic Polarizability, Optical Basicity and XPS Spectra of Sb_2O_3-B_2O_3 Glasses. *J. Non-Cryst. Solids* **2000**, *272*, 1.
(43) Hanafi Z. M., Ismail F. M. *NIST X-ray Photoelectron Spectroscopy Database*. http://srdata.nist.gov/xps/EngElmSrchQuery.aspx?EType=PE&CSOpt=Retri_ex_dat&Elm=Sb (accessed Feb 25, 2014).
(44) Barin, I.; Sauert, F.; Schultze-Rhonhof, E.; Sheng, W. S. *Thermochemical Data of Pure Substances*, 2nd ed.; VCH: Weinheim, Germany, 1993; pp 1443–1451.
(45) Vadapoo, R.; Krishnan, S.; Yilmaz, H.; Marin, C. Electronic Structure of Antimony Selenide (Sb_2Se_3) from GW Calculations. *Phys. Status Solidi (b)* **2011**, *248*, 700.
(46) Konstantatos, G.; Howard, I.; Fischer, A.; Hoogland, S.; Clifford, J.; Klem, E.; Levina, L.; Sargent, E. H. Ultrasensitive Solution-Cast Quantum Dot Photodetectors. *Nature* **2006**, *442*, 180.
(47) Konstantatos, G.; Levina, L.; Fischer, A.; Sargent, E. H. Engineering the Temporal Response of Photoconductive Photodetectors via Selective Introduction of Surface Trap States. *Nano Lett.* **2008**, *8*, 1446.
(48) Konstantatos, G.; Sargent, E. H. PbS Colloidal Quantum Dot Photoconductive Photodetectors: Transport, Traps, and Gain. *Appl. Phys. Lett.* **2007**, *91*, 173505.
(49) Morkel, M.; Weinhardt, L.; Lohmuller, B.; Heske, C.; Umbach, E.; Riedl, W.; Zweigart, S.; Karg, F. Flat Conduction-Band Alignment at the CdS/$CuInSe_2$ Thin-Film Solar-Cell Heterojunction. *Appl. Phys. Lett.* **2001**, *79*, 4482.